Acta Geotechnica
https://doi.org/10.1007/s11440-024-02326-8

RESEARCH PAPER

Effects of subgrade spatial variability on critical strains and effectiveness of geogrid reinforcement in flexible pavement

Li Xiao[1] · Jianfeng Xue[1]

Received: 26 July 2023 / Accepted: 12 March 2024

Abstract

The objective of this study is to assess the impact of spatial variability in the subgrade layer on the critical response of pavements and the effectiveness of geogrid reinforcement, employing the random field finite difference analysis (RFFDA). A comprehensive parametric study was conducted to examine the influence of two crucial factors: the coefficient of variation (COV_E) and scale of fluctuation (SOF) of the subgrade modulus. Further investigation was conducted to uncover the statistical and mechanical mechanisms underlying the impact of subgrade spatial variability with emphasis on the critical strain distributions and their correlation with both the overall modulus and the local spatial variability of the key influence zone. Furthermore, this study explored the influence of subgrade spatial variability on the effectiveness of geogrid in reducing critical strains, considering various placement positions and geogrid moduli. The following main conclusions are drawn: (a) subgrade spatial variability has a substantial amplifying effect on critical pavement strains due to low modulus dominating effect, (b) there exists a worst value of SOF that results in the most unfavorable statistics of critical subgrade strain, (c) the effect of subgrade spatial variability on critical subgrade strain is more pronounced compared to its effect on critical asphalt strain, (d) the mean value of critical subgrade strain in RFFDA can be significantly underestimated when assuming fixed location for the strain, and (e) the effectiveness of geogrid in reducing critical strains is impacted by subgrade spatial variability, with the impact varying with the type of critical strain and geogrid location. Specifically, when placed at the base course–subgrade interface, the ability of geogrid to reduce critical subgrade strain is significantly compromised due to the subgrade spatial variability.

Keywords Geogrid reinforcement · Pavement · Random field · Spatial variability · Subgrade

Abbreviations

AASHTO	American Association of State Highway and Transportation Officials
CBR	California Bearing Ratio
COV	Coefficient of variation
DCP	Dynamic cone penetrometer
IRI	International roughness index
KIZ	Key influence zone
LWD	Light weight deflectometer
ME	Mechanistic-empirical
RFFDA	Random field finite difference analysis
SAR	Strain alleviating ratio
SOF	Scale of fluctuation
G1	Geogrid with 2500 kN/m secant stiffnesses (J) at 2% of strain
G2	Geogrid with 5000 kN/m secant stiffnesses (J) at 2% of strain
L1	Asphalt–base course interface
L1-2	Mid-depth of base course
L2	Base course–subgrade interface
G_L1	Geogrid reinforcement with geogrid (G1 or G2) placed at L1
G_L2	Geogrid reinforcement with geogrid (G1 or G2) placed at L2
G_L1-2	Geogrid reinforcement with geogrid (G1 or G2) placed at L1-2
E	Subgrade modulus
$E(\boldsymbol{X_i})$	Vector of random variables for the subgrade modulus
E_{Local}	Arithmetic mean modulus of meshes in the KIZ

✉ Jianfeng Xue
jianfeng.xue@unsw.edu.au

Li Xiao
li.xiao@unsw.edu.au

[1] School of Engineering and Technology, The University of New South Wales, Campbell 2612, Australia

Published online: 12 April 2024

E_{det}	Deterministic subgrade modulus
μ_E	Mean value of subgrade modulus
COV_E	Coefficient of variation of subgrade modulus
$\text{COV}_{E,1}$	Coefficient of variation of E_{Local}
$\text{COV}_{E,2}$	Average coefficient of variation of the moduli in the six meshes of the KIZ
$\zeta_{\ln E}$	Mean value of the normal distribution of $\ln(E)$
$\lambda_{\ln E}$	Standard deviation of the normal distribution of $\ln(E)$
δ_x	Horizontal scale of fluctuation
δ_y	Vertical scale of fluctuation
D	Width of the uniform contact stress used to simulate the tire pressure
R_L	Length ratio of scale of fluctuation (SOF) to the width of the uniform contact stress (D)
R_{A}	Strain amplification ratio
$R_{D,\max}$	Deviation ratio of maximum critical strain
$R_{D,\min}$	Deviation ratio of minimum critical strain
$\varepsilon_h^{\text{ac}}$	Maximum horizontal tensile strain at the bottom of asphalt layer
$\varepsilon_v^{\text{sub}}$	Maximum vertical compressive strain on the top of subgrade layer
P0	Position for $\varepsilon_h^{\text{ac}}$ in deterministic scenario
Q0	Position for $\varepsilon_v^{\text{sub}}$ in deterministic scenario
$\varepsilon_{h,P0}^{\text{ac}}$	Horizontal asphalt strain at P0 in a spatially variable case
$\varepsilon_{v,Q0}^{\text{sub}}$	Vertical subgrade strain at Q0 in a spatially variable case
$\varepsilon_{v,\text{det}}^{\text{sub}}$	Critical subgrade strain in deterministic scenario
$\overline{\varepsilon}$	Mean value of the critical asphalt or subgrade strain in a spatially variable case
ε_{det}	Critical asphalt or subgrade strain in the deterministic case
σ_v^{sub}	Average vertical stress transmitted to the top of KIZ in a spatially variable case
$\sigma_{v,\text{det}}^{\text{sub}}$	Vertical stress transmitted to the top of KIZ in a deterministic variable case

1 Introduction

The subgrade layer is the natural or prepared soil layer beneath the pavement structures, and it plays a crucial role in providing the support and stability required for the overlying pavement. However, the level of support as characterized by the subgrade strength or modulus can vary spatially due to a combination of factors such as natural deposition processes, variation in construction quality and environmental change. Spatial variability in the subgrade layer can have significant impacts on pavement performance. Non-uniform settlement and deformation of the pavement may arise due to this variability [19], resulting in undesirable and excessive pavement distress such as cracking, rutting, and roughness [37]. Furthermore, localized bearing capacity failure may also occur in regions where the subgrade is very weak or soft, leading to the ingress of moisture and the contamination of the aggregate base material with underlying soft subgrade soil. All these consequences can exacerbate the risk of premature failure of the pavement system.

Spatial variability is a significant contributor to material uncertainty in geotechnical engineering [32]. It can be effectively characterized using random field theory, primarily through two key parameters: the coefficient of variation (COV) and the scale of fluctuation (SOF). The COV describes the extent of dispersion in material properties. The SOF, which characterizes the pattern of property dispersion, is the distance at which the correlation between two points in the field decays to a negligible level. The random field finite element analysis (RFFEA), or the random field finite difference analysis (RFFDA), both of which integrate numerical simulation with random field theory and Monte Carlo Simulation, are probabilistic frameworks widely employed to characterize the spatial variability of materials and assess its statistical impact on the structural response [11, 19, 20, 22, 23, 27, 41].

Numerous studies have investigated the influence of subgrade spatial variability on the pavement response with the two probabilistic frameworks. Lua and Sues [27] performed a comprehensive probabilistic analysis that accounted for various uncertainties, including spatial variability arising from the asphalt layer and foundation layers (i.e., the base and subgrade layers). They concluded that ignoring spatial variability can lead to inaccurate prediction of pavement life. Ali et al. [4] examined the impact of subgrade spatial variability on pavement responses and revealed that the rutting life is more sensitive to the subgrade spatial variability as opposed to fatigue life. Vaillancourt et al. [37] investigated the effect SOF of subgrade stiffness on the roughness of flexible pavements, as quantified by the International Roughness Index (IRI). They found that SOF had a direct impact on the wavelength of the resulting deformations and the IRI value. Alhasan et al. [3] employed geospatial models to define the spatial variability and systematic measurement errors of base and subgrade layers and consequently established a mechanistic-empirical (ME) pavement performance model based on reliability analysis. They concluded that: (1) when performing risk and reliability analysis, it is essential to distinguish the inherent spatial variability from other uncertainties and (2) the location of critical responses can

be different from the deterministic situation described in the ME pavement design guides such as AASHTO [1]. Choudhuri and Chakraborty [13] investigated how the horizontal and vertical SOF of the subgrade soil affect the pavement bearing capacity using an anisotropic random field.

The above studies focus on the influence of spatial variability in subgrade layers on pavement performance, consistently revealing the adverse impact of such variability on the structural response of pavements. However, there are limited studies effectively delving into the statistical and mechanical mechanisms behind these effects. Additionally, it remains uncertain whether there exists a specific "worst" SOF that leads to the most unfavorable statistical consequences for pavement response.

Moreover, the impacts of spatial variability in subgrade layers have received scant attention in various practical scenarios commonly encountered in practice. For example, the use of geogrid reinforcement is a widely adopted practice in pavement engineering due to its potential to improve pavement performance, such as reducing critical strains, mitigating rut depth and crack development [15, 16, 21]. However, the impact of subgrade spatial variability on the efficacy of geogrid reinforcement remains largely unexplored. The effectiveness of geogrid reinforcement relies on various design variables, such as the type and properties of geosynthetic [10, 33], the placement position of geosynthetic [29, 43], the thickness of design section [15], the loading magnitude and conditions [10, 33], and the subgrade strength [9, 16, 39]. Correia et al. [16] found that the reduction in the asphalt surface vertical displacements resulting from the geogrid-reinforced asphalt layers was more significant for pavement on comparatively weak subgrades. Notably, contradictory findings have been reported regarding the impact of subgrade strength on the effectiveness of geogrid reinforcement used in the base course layer. Cancelli et al. [9] observed a reduction in the reinforcement benefit as subgrade strength increases, while Webster [39] found that a higher California Bearing Ratio (CBR) in the subgrade resulted in a greater reinforcement benefit. Given the limited number of studies available, it remains inconclusive whether or not the geogrid reinforcement in the base course layer is more beneficial on a weaker subgrade. Additionally, the impacts of weak subgrade on the geogrid reinforcement placed at other positions within the pavement system have not been adequately explored. The situation becomes more complex when considering a subgrade with spatial variability, as it introduces different strain and stress distributions within the multilayer pavement system compared to deterministic conditions. These variations can significantly influence the effectiveness of geogrid reinforcement. Nevertheless, it remains unclear whether the subgrade spatial variability enhances or hampers the geogrid reinforcement. This knowledge gap highlights the necessity for further research to address these issues.

This study investigates the effects of subgrade spatial variability on critical pavement responses and the effectiveness of geogrid reinforcement using the random field finite difference analysis (RFFDA). The critical pavement response variables analyzed are the maximum horizontal tensile strain at the bottom of the asphalt layer ($\varepsilon_h^{\mathrm{ac}}$) and the maximum vertical compressive strain on top of the subgrade layer ($\varepsilon_v^{\mathrm{sub}}$). These strains are normally used to estimate the pavement fatigue life (using $\varepsilon_h^{\mathrm{ac}}$) and rutting life (using ε_v^{sub}), respectively, i.e., the respective number of load repetitions for fatigue and rutting failures [1, 7]. To avoid the complex coupling effect of different sources of uncertainties, only the subgrade modulus is considered as spatially variable, assuming all other parameters to be homogeneous and deterministic. Parametric studies were conducted to examine the effects of two key influencers, namely the coefficient of variation (COV_E) and the scale of fluctuation (SOF) of subgrade modulus. Further investigation was conducted to uncover the statistical and mechanical mechanisms underlying the impact of subgrade spatial variability by analyzing the critical strain distributions and their correlations with both the overall modulus and the local spatial variability of the key influence zone. Finally, the influence of subgrade spatial variability on the effectiveness of geogrid reinforcement in mitigating critical strains is also explored, considering various locations and moduli of the reinforcements.

2 Random field finite difference analysis (RFFDA)

2.1 Finite difference model of the pavement structure

A typical three-layer pavement structure subjected to a load of 53 kN from a single-tired single-axle was chosen for analysis in this study. The load is represented by a uniform contact stress of 800 kPa over two areas with a width of D = 204.8 mm spaced by 2130 mm [7]. Though the deformation of pavements under wheel loading is a 3D problem, 2D pavement models are often employed in numerical simulations for simplification [6, 16, 21, 28]. To enhance the computational efficiency of RFFDA, the pavement structure is simulated with a plane strain model by constraining it to a 2D plane in FLAC3D software. As shown in Fig. 1, the mesh sizes of the pavement model are 0.05 m horizontally and vary vertically depending on their distance from the loading and the thickness of the layer.

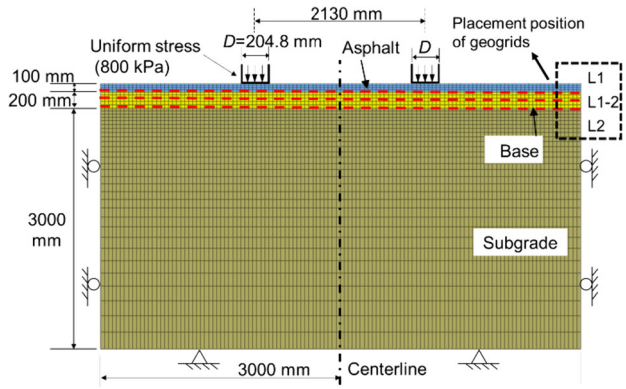

Fig. 1 Finite difference model of the three-layered pavement

Table 1 Material properties of the pavement model [7]

Material	Asphalt layer	Base layer	Subgrade layer
Thickness (mm)	100	200	3000
Young's modulus (MPa)	4000	200	60
Poisson's ratio	0.4	0.35	0.28
Cohesion (kPa)	–	5	30
Friction angle (°)	–	40	25
Unit weight (kN/m^3)	24	20	18.2

The vertical boundaries are fixed in horizontal directions and the bottom is fixed in all directions. The base and subgrade layers are simulated with the Mohr–Coulomb constitutive model, and the asphalt layer with a linear elastic material [5, 16, 31]. The material properties are listed in Table 1.

In deterministic scenarios, the critical strains (ε_h^{ac} and ε_v^{sub}) would occur along the vertical axis directly beneath the tire pressure [7]. However, in probabilistic analysis incorporating spatial variability, the occurrence of critical strains may not necessarily align with the locations observed in the deterministic scenarios. This issue will be thoroughly investigated and discussed in the following sections.

To investigate the impact of subgrade spatial variability on geogrid reinforcement, this study incorporates six types of reinforcement arrangements. These arrangements consider two levels of geogrid stiffness (G1 and G2) and three placement positions (L1, L1-2, L2). Specifically, L1 represents the location at the interface between the asphalt and base course, L1-2 the middle of the base course, and L2 the interface between the base course and subgrade. The secant stiffnesses (J) at 2% of strain are 2500 kN/m and 5000 kN/m for G1 and G2, respectively. Linear shear behavior is assumed for the interfaces between the geogrid and the surrounding materials.

Table 2 lists the detailed simulation scheme and the interface properties of the six geogrid reinforcements. These geogrid parameters were determined based on existing field and laboratory tests [2, 10, 14, 30]. The shear moduli of the soil/aggregate–geogrid interface are influenced by multiple factors [10, 34], including geogrid type, interface type, vertical pressure on the geogrids, and even environmental temperature. These factors are not examined in this study but will be explored in future research to explore their possible impact on geogrid's strain alleviation capacity under subgrade spatial variability. The geogrids are simulated with geogridSEL in FLAC3D.

2.2 Validation of finite difference modeling

Correia et al. [16] performed 2D finite element analyses on a large-scale paved model test, and the results showed the efficiency of using a 2D model to simulate the 3D problem when proper models and material properties are adopted. The 3D large-scale paved model test by Correia et al. [16] was employed to check the validity of the constitutive models used in this study. Figure 2 shows the finite difference model of the test under plane strain assumption in FLAC3D software. The material properties reported by Correia et al. [16] are used in the validation simulation.

Table 2 Simulation programs of the six reinforcement arrangements and interface properties of the geogrids [2, 10, 14, 30]

Simulation program	Reinforcement type	Reinforcement location	Interface properties		
			Shear stiffness, K_s (MPa/m)	Cohesion (kPa)	Friction angle (°)
G1_L1	G1	L1: Asphalt–base course interface	600	300	45
G2_L1	G2		1200	300	45
G1_L1-2	G1	L1-2: Middle of base course	600	5	40
G2_L1-2	G2		1200	5	40
G1_L2	G1	L2: Base course–subgrade interface	600	30	25
G2_L2	G2		1200	30	25

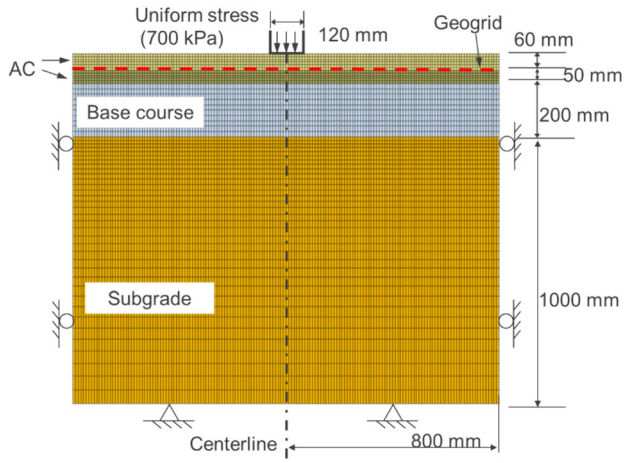

Fig. 2 Finite difference model of the large-scale paved model test by Correia et al. [16]

The maximum asphalt surface displacement reported in the test was 1.8 mm [16]. The numerical prediction shows a close result of 1.9 mm, representing a 5% deviation. Figure 3 compares the experimental and predicted vertical stress distribution across pavement layers and the geogrid strain distribution. Figure 3a demonstrates that the finite difference model accurately predicted the vertical stress observed in the experiment. A good match has been observed at four critical locations: the interface between asphalt layers, the bottom of the lower asphalt layer, the middle of the base course, and 10 cm below the top of the subgrade layer. In Fig. 3b, the strain distribution of the numerical model aligns well with the experimental results. The geogrid strain peaks right beneath the wheel load center and decreases with distance from the wheel load. However, discrepancies between numerical predictions and experimental findings are noticeable near the wheel load and in regions extending 400 mm to 600 mm from it. These inconsistencies might stem from the limitations of linear elastic models in simulating volumetric changes in AC material and the nonlinear behavior of geogrids [26]. Despite this, the numerical model well predicts both the magnitude and location of the peak geogrid strain. Additionally, it shows no geogrid mobilization beyond 300 mm from the wheel load, aligning with the experimental findings.

Thus, the 2D finite difference model accurately predicted the key performance of the 3D large-scale paved model test. This validation confirms the efficacy of the finite difference modeling procedure, including the plane strain assumption and constitutive models, to represent the actual 3D geogrid-reinforced pavement model.

2.3 Modeling and discretization of random field

The spatial variability of subgrade modulus is simulated with a continuous and stationary 2D random field. This field is characterized by a vector of random variables $E(\boldsymbol{X_i})$ following the lognormal distribution with its mean μ_E = 60 MPa and different coefficients of variation (COV_E). The lognormal distribution is chosen to avoid the generation of negative material properties [14]. The exponential autocorrelation function adopted by Huang et al. [24] is used to define the correlation of the random variables $E(\boldsymbol{X_i})$ at two locations:

$$\rho(x,y) = \exp(-2|x|/\delta_x)\exp\left(-2|y|/\delta_y\right) \quad (1)$$

where δ_x represents the horizontal scale of fluctuation (SOF), while δ_y represents the vertical SOF. The variables x and y denote the relative horizontal and vertical coordinates of any two points, respectively. This study focuses only on the 2D isotropic random field of the subgrade layer. The spatial variation along the alignment direction is not considered. Consequently, the horizontal and vertical scale of fluctuation (δ_x and δ_y) are assumed to be equal and will be collectively referred to as SOF henceforth.

The random field $E(\boldsymbol{X_i})$ is obtained through two steps:

(a) Generating a group of normally distributed random field $G(\boldsymbol{X_i})$ using zero mean, unit variance, an

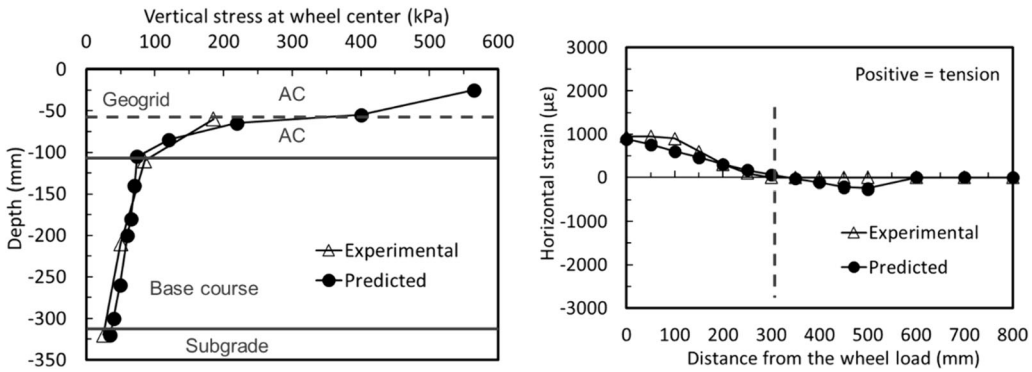

Fig. 3 Comparison of experimental and predicted results: **a** vertical stress distribution; **b** geogrid strain distribution

autocorrelation function $\rho(x, y)$, and an appropriate Monte Carlo simulation number. The Karhunen–Loève expansion method is chosen to generate the random field for its excellent approximation to the original random field and computational efficiency in high-dimensional problems [25, 42].

(b) Deriving the lognormally distributed random field $E(\boldsymbol{X_i})$ from $G(\boldsymbol{X_i})$ using the following transformation equations:

$$\zeta_{\ln E} = \sqrt{\ln(1 + \mathrm{COV}_E^2)} \tag{2}$$

$$\lambda_{\ln E} = \ln \mu_E - \frac{1}{2}\zeta_{\ln E}^2 \tag{3}$$

$$E(\boldsymbol{X_i}) = exp[\lambda_{\ln E} + \zeta_{\ln E} G(\boldsymbol{X_i})] \tag{4}$$

where $\zeta_{\ln E}$ and $\lambda_{\ln E}$ are the mean and standard deviation of the normal distribution of $\ln(E)$, respectively.

Generally, the required number of Monte Carlo simulations depends on precision requirements and available computational resources. A convergence analysis was conducted by progressively increasing the simulation number from 20 to 1400 in RFFDA with COV_E =0.5 and SOF = 0.25 m. It was observed that, when the number of simulations exceeds 200, the mean and COV of both critical subgrade strain ($\varepsilon_v^{\mathrm{sub}}$) and critical asphalt strain ($\varepsilon_h^{\mathrm{ac}}$) stabilize with an error percentage below 1.5%. Hence, 200 Monte Carlo simulations are utilized for subsequent RFFDA.

2.4 Key influence zone (KIZ)

In probabilistic analysis, the magnitudes of critical strains, particularly $\varepsilon_v^{\mathrm{sub}}$, exhibit variations among different realizations due to the spatially variable modulus in the subgrade. The magnitude of $\varepsilon_v^{\mathrm{sub}}$ is primarily governed by the magnitude and spatial distribution of subgrade modulus in the vicinity of its critical location, known as the key influence zone (KIZ) for $\varepsilon_v^{\mathrm{sub}}$. Outside the KIZ, the distribution of subgrade modulus makes an insignificant contribution to the difference of pavement responses between spatially variable and deterministic cases, as it is statistically equivalent to the deterministic case and far away from the critical location.

To locate the KIZ, Fig. 4 presents the contour of vertical compressive stress in the subgrade within 1 m of the base's underside. At a horizontal distance of 0.15 m (equivalent to 0.75D) from the loading centerline at the subgrade top, the stress reduces to less than 60% of the maximum value. This indicates that the critical subgrade strain and stress are predominantly within a width region of 0.3 m (i.e., 1.5D) beneath the loading area. Therefore, the region depicted in Fig. 4, with a width of 1.5D and a thickness of 35 mm, is

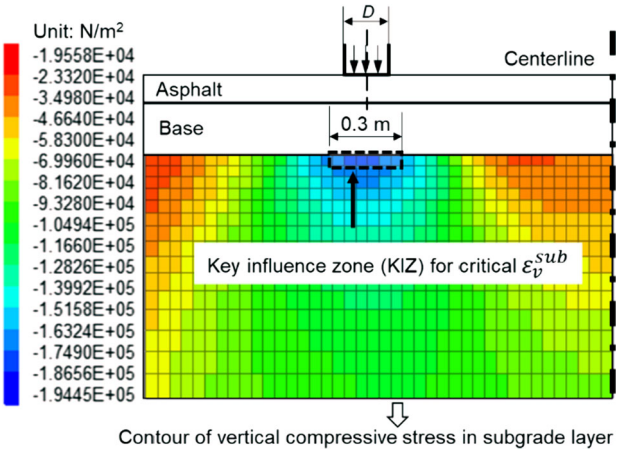

Fig. 4 Key influence zone (KIZ) for the critical subgrade strain

identified as the KIZ. The random distribution of Young's modulus of the subgrade may slightly affect the local mean values in the KIZ, but may not greatly change the ratio between the moduli of the base course and the subgrade within the KIZ. The size of the KIZ is mainly affected by the ratio between the asphalt, base course and subgrade moduli, and the thicknesses of the asphalt and the base course layers. As long as the ratios and the thicknesses do not vary too much, the size of KIZ will not vary significantly. For simplification, in the analyses, the size of the KIZ was kept constant in all the analyses. However, if the thickness and moduli of the pavement layers significantly differ from those in Table 2, the dimensions of KIZ may change accordingly.

To quantify the overall modulus of the KIZ, a local modulus, E_{Local}, is defined as the arithmetic mean modulus of meshes in the KIZ. The statistics of critical strains in spatially variable cases are significantly influenced by E_{Local} and the internal spatial variability within the KIZ. Further elaboration on this aspect will be provided in subsequent sections.

2.5 Parametric study

A parametric study was conducted to explore how changes in the subgrade spatial variability affect the critical pavement responses ($\varepsilon_h^{\mathrm{ac}}$ and $\varepsilon_v^{\mathrm{sub}}$). Two key input parameters, namely the coefficient of variation (COV_E) and the scale of fluctuation (SOF) of the subgrade modulus, are systematically varied within predefined ranges. The coefficient of variation is site-specific and can vary depending on factors such as the soil type, testing methods employed, and the inherent variability in the subgrade material [18, 32, 36, 40]. Timm et al. [36] reported a COV_E ranging from 5 to 50%. White et al. [40] found the COV_E to be within 38–97% based on the light weight deflectometer

(LWD) tests and dynamic cone penetrometer (DCP) tests. Phoon and Kulhawy [32] revealed COV_E ranging from 9 to 92% for various types of soil. Considering the typical range, this study assumes COV_E values of 0.3 and 0.5 for the parametric analysis. In comparison, information on SOF is relatively limited.

Typical values of SOF can range from 0.1 to 60 m for a variety of geotechnical parameters [8, 32]. The strength and variability of subgrade soil within 1 m below the base course is usually assessed to determine the subgrade design parameters (such as modulus and CBR), and the subgrade within 1 m of the underside of the base often shows vertical stratification [7]. To capture the stratifications within this 1 m depth, the SOF of the subgrade layer adopted in the simulations need to be less than 1 m. When SOF is set larger than 1 m, it cannot capture the spatial variability within this crucial 1 m depth subgrade region. A prior study conducted by Lua and Sues [27] adopted SOFs ranging from 0.1 to 1 m for investigating the impact of subgrade spatial variability on pavement performance. Therefore, the SOF is selected between 0.1 and 1 m in this study.

Table 3 presents the parameter combinations for 24 spatial variable cases with SOF ranging from 0.1–1.0 m and COV_E values of 0.3 or 0.5. A length ratio $R_L = \mathrm{SOF}/D$ is defined to assess the relative length of SOF over the loading areas. Specifically, the SOF of Case 1–3 and Case 2–3 equals D, the width of the loading area; and the SOF in Case 1–5 and Case 2–5 equals $1.5D$, the widths of KIZ. Figure 5 shows 6 realizations of random fields with $COV_E = 0.5$ at different SOF levels. All SOFs considered in this study exceed the maximum subgrade mesh size within 1 m below the base layer, ensuring that the discretization of the random field does not introduce substantial inconsistency with the continuous solution in this region [12].

Table 3 Parameter combinations of the 24 spatial variable cases

Group 1 COV_E=0.3	Group 2 COV_E=0.5	SOF(m)	R_L = SOF/D
Case 1–1	Case 2–1	0.10	0.50
Case 1–2	Case 2–2	0.15	0.75
Case 1–3	Case 2–3	0.20	1.00
Case 1–4	Case 2–4	0.25	1.25
Case 1–5	Case 2–5	0.30	1.50
Case 1–6	Case 2–6	0.35	1.75
Case 1–7	Case 2–7	0.40	2.00
Case 1–8	Case 2–8	0.50	2.50
Case 1–9	Case 2–9	0.60	3.00
Case 1–10	Case 2–10	0.70	3.50
Case 1–11	Case 2–11	0.80	4.00
Case 1–12	Case 2–12	1.00	5.00

3 Result and analysis

3.1 Effect of spatial variability on the statistics of critical strains

Table 4 lists the statistics of critical strains for the 24 spatial variable cases in Table 3, including the mean values, COVs, and extremes. The corresponding deterministic values are 1.283 millistrain for ε_h^{ac} and 3.709 millistrain for ε_v^{sub}. All the strains in Table 4 are within reasonable range of pavements [7].

Subsequent sections will assess the influence of SOF and COV_E on these statistics and the locations of critical strains. The analysis aims to elucidate the statistical and mechanical mechanisms underlying the impacts of subgrade spatial variability.

3.1.1 Critical locations

This section aims to investigate and assess the influence of subgrade spatial variability on the critical locations of the maximum tensile strain in the asphalt layer (ε_h^{ac}) and the maximum vertical compressive strain in the subgrade layer (ε_v^{sub}). Figure 6 shows the potential critical positions, where P0 and Q0 represent the critical positions for ε_h^{ac} and ε_v^{sub} in deterministic scenarios, respectively. Note that P0 is not located at the centerline of the loading area, as the centerline of the loading area differs from the centerline of the pavement model.

Figure 7 presents the distribution of critical subgrade strain at different locations for different values of SOF and COV_E. In the majority of cases, more than 50% of realizations show a critical subgrade strain occurring away from Q0, suggesting that assuming Q0 as the critical location may result in an undervalued ε_v^{sub} with a likelihood of over 50%. Additionally, when SOF is 0.3 m, i.e., the width of the KIZ, the number of realizations with ε_v^{sub} at Q0 reaches the minimum regardless of COV_E. When SOF increases beyond 0.3 m, the number of realizations with a Q0 critical strain tends to increase. This can be attributed to the homogenization of the KIZ, as SOF transitions from a value smaller than $1.5D$ to a significantly larger value. On the other hand, the comparison of Fig. 7a and b indicates that, at a larger COV_E, the likelihood of the critical subgrade strain occurring at Q0 reduces.

It is anticipated that the critical locations of ε_h^{ac} would be relatively unaffected by the subgrade spatial variability. This is attributed to the spatial averaging effect, where

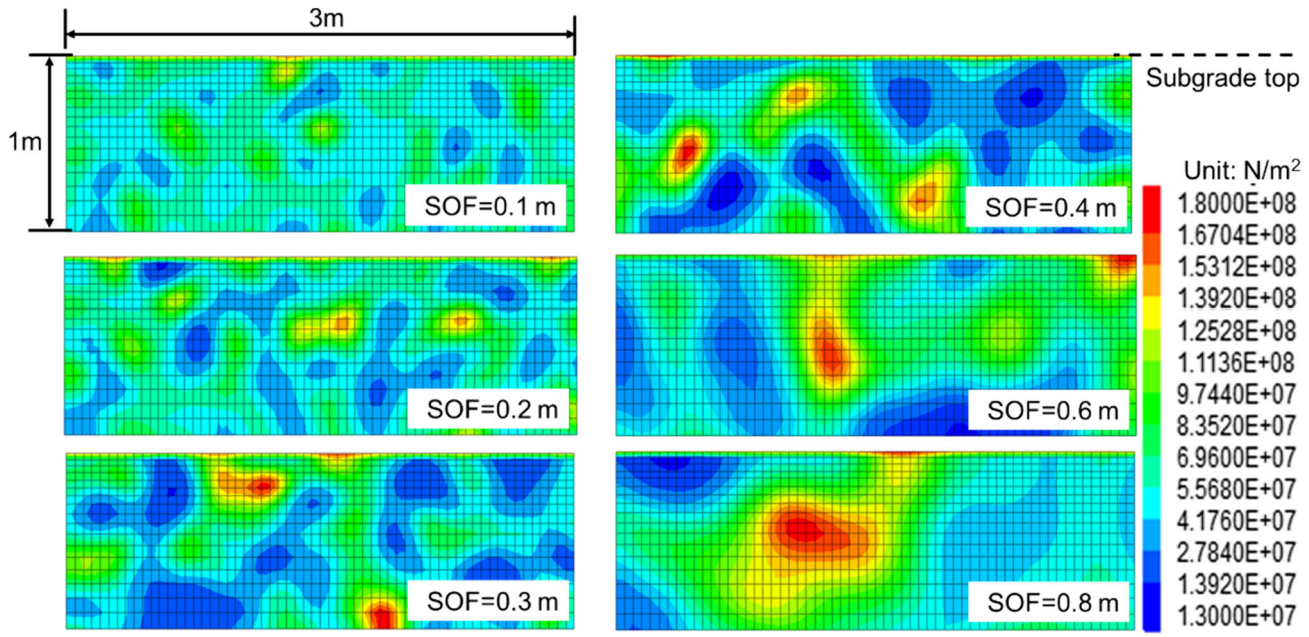

Fig. 5 Random fields of Young's modulus in the subgrade layer of different SOFs (COV_E = 0.5)

larger areas or longer distances tend to smooth out local variations, resulting in a more homogeneous and deterministic response [38]. This expectation is confirmed by Fig. 8. For COV_E values of 0.3 and 0.5, P0 is determined as the critical location in 99% and 97% of the realizations, respectively. Noticeable deviations from P0 are observed only when both SOF and COV_E are of considerably high values, as shown in Fig. 8b.

Overall, subgrade spatial variability has a much greater impact on the critical locations of $\varepsilon_v^{\text{sub}}$ compared to $\varepsilon_h^{\text{ac}}$. This effect highlights the potential underestimation of $\varepsilon_v^{\text{sub}}$ when assuming a fixed location for maximum subgrade strain in RFFDA. The upcoming section will evaluate the extent of underestimation resulting from this assumption.

3.1.2 Mean values of critical strains

Since the magnitudes of critical strains vary among different realizations due to the spatially variable modulus in the subgrade, their mean values could be different from their deterministic counterparts. To assess the impact of spatial variability on the mean critical strains, a relative strain amplification ratio R_A is defined as:

$$R_A = (\bar{\varepsilon}/\varepsilon_{\text{det}} - 1) \times 100\% \quad (5)$$

where $\bar{\varepsilon}$ denotes the mean value of the critical strains in a spatially variable case, and ε_{det} represents the corresponding critical strains in the deterministic case.

Figure 9a shows how the variation of SOF affects R_A for $\varepsilon_v^{\text{sub}}$ under different values of COV_E. In the figure, two kinds of critical subgrade strain are presented for each case: the actual critical strain ($\varepsilon_v^{\text{sub}}$) and the strain at Q0 ($\varepsilon_{v,Q0}^{\text{sub}}$). It shows that the impact of SOF on R_A is more pronounced for $\varepsilon_v^{\text{sub}}$ compared to $\varepsilon_{v,Q0}^{\text{sub}}$. For $\varepsilon_v^{\text{sub}}$, the value of R_A increases as SOF increases from 0.05 to approximately 0.3 m and then decreases as SOF increases from 0.3 to around 0.7 m. Subsequently, R_A remains relatively stable. On the other hand, R_A for $\varepsilon_{v,Q0}^{\text{sub}}$ increases as SOF increases from 0.05 m to approximately 0.3 m and then stabilizes. Notably, the maximum R_A values for $\varepsilon_v^{\text{sub}}$ and $\varepsilon_{v,Q0}^{\text{sub}}$, as well as the greatest discrepancy between R_A for $\varepsilon_v^{\text{sub}}$ and $\varepsilon_{v,Q0}^{\text{sub}}$, are observed when SOF is approximately 0.3 m. Specifically, when SOF = 0.3 m and $COV_E = 0.5$, the mean values of $\varepsilon_v^{\text{sub}}$ and $\varepsilon_{v,Q0}^{\text{sub}}$ are increased by 22% and 13%, respectively, relative to the deterministic strain. This indicates that the amplifying effect of subgrade spatial variability on $\varepsilon_{v,Q0}^{\text{sub}}$ can be as low as 60% of that on $\varepsilon_v^{\text{sub}}$. Hence, the subgrade strains extracted at Q0 might not represent the actual critical subgrade strains and can result in a significant underestimation of the amplifying impact resulting from subgrade spatial variability. These findings highlight the need for careful determination of the critical strain location for subgrade strain when considering the subgrade spatial variability, particularly in situations where SOF is approximately 1.5*D*.

Figure 9b depicts the variation of R_A for ε_h^{ac} with SOF. The value of R_A initially increases with increasing SOF and maximizes at SOF = 0.4 m (i.e., 2*D*), after which it remains relatively stable. Compared with $\varepsilon_v^{\text{sub}}$, the impact of SOF on mean ε_h^{ac} is minimal, with R_A values ranging from

Table 4 Statistics of critical strains of the 24 spatial variable cases

Case No.	Statistics for ε_h^{ac}				Statistics for ε_v^{sub}			
	Mean	COV	Maximum	Minimum	Mean	COV	Maximum	Minimum
Case 1–1	1.305	0.6%	1.331	1.287	3.838	6.6%	4.610	3.197
Case 1–2	1.309	1.0%	1.352	1.269	3.894	10.5%	5.471	2.953
Case 1–3	1.314	1.3%	1.355	1.266	3.952	13.1%	5.432	2.754
Case 1–4	1.317	1.5%	1.387	1.276	3.976	14.8%	5.347	2.404
Case 1–5	1.316	1.9%	1.393	1.248	4.002	16.4%	6.545	2.525
Case 1–6	1.317	2.1%	1.408	1.253	4.008	16.7%	5.801	2.424
Case 1–7	1.318	2.1%	1.388	1.242	3.975	18.1%	6.404	2.588
Case 1–8	1.317	2.6%	1.415	1.228	3.953	19.4%	6.904	2.298
Case 1–9	1.318	3.1%	1.472	1.230	3.926	18.1%	6.642	2.504
Case 1–10	1.317	3.7%	1.428	1.179	3.904	16.4%	5.711	2.362
Case 1–11	1.316	3.7%	1.453	1.187	3.902	17.7%	5.954	2.533
Case 1–12	1.317	4.6%	1.532	1.155	3.907	18.5%	6.140	2.058
Case 2–1	1.347	0.9%	1.384	1.317	4.083	9.7%	5.190	2.915
Case 2–2	1.360	1.5%	1.417	1.309	4.201	17.2%	6.887	2.490
Case 2–3	1.370	2.1%	1.452	1.289	4.427	20.8%	7.351	2.573
Case 2–4	1.374	2.6%	1.501	1.274	4.496	24.1%	7.973	2.300
Case 2–5	1.378	3.0%	1.499	1.239	4.524	28.1%	8.838	1.935
Case 2–6	1.379	3.7%	1.543	1.266	4.463	26.8%	8.841	2.206
Case 2–7	1.380	3.4%	1.529	1.273	4.424	27.9%	9.713	2.320
Case 2–8	1.377	4.1%	1.532	1.221	4.346	27.6%	9.390	2.152
Case 2–9	1.378	5.3%	1.575	1.215	4.304	26.1%	8.216	1.909
Case 2–10	1.379	6.0%	1.633	1.196	4.248	26.8%	7.440	1.775
Case 2–11	1.376	5.8%	1.615	1.227	4.262	28.3%	8.433	2.063
Case 2–12	1.372	7.0%	1.661	1.165	4.239	29.2%	8.469	1.946

The unit for the critical strains is millistrain

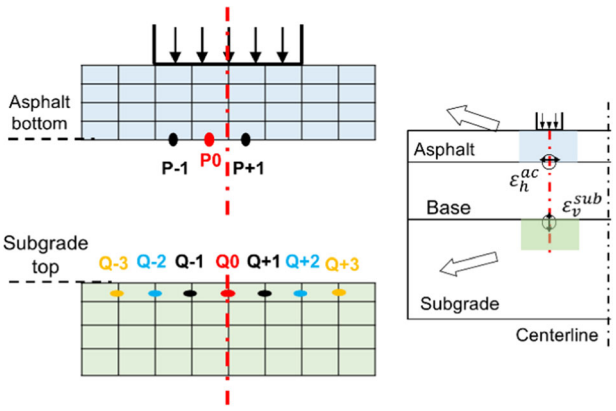

Fig. 6 Possible critical locations for ε_h^{ac} and ε_v^{sub} in spatial variable cases

1.8% to 2.7% for COV_E = 0.3 and from 5.0% to 7.6% for COV_E = 0.5. Furthermore, there is a negligible discrepancy between ε_h^{ac} and the tensile strain at P0 ($\varepsilon_{h,P0}^{ac}$), which confirms that the critical location of ε_h^{ac} is relatively unaffected by the subgrade spatial variability.

The underestimation of critical strains, particularly for ε_v^{sub}, is substantial when assuming the same critical locations in spatial variable cases as in deterministic case. Therefore, the actual critical strains, rather than solely those at the P0 or Q0 positions, will be considered for the analysis in the subsequent sections.

3.1.3 Coefficient of variation (COV) of the critical strains

Figure 10 shows the variations in the coefficient of variation (COV) for the critical strains as SOF increases under different values of COV_E. The figure reveals that increasing spatial variability, as characterized by the higher COV_E, leads to an elevated COV for the critical strains, particularly for ε_v^{sub}. This observation aligns with Ali et al. [4] who found a proportional relationship between the variability of pavement response and that of the

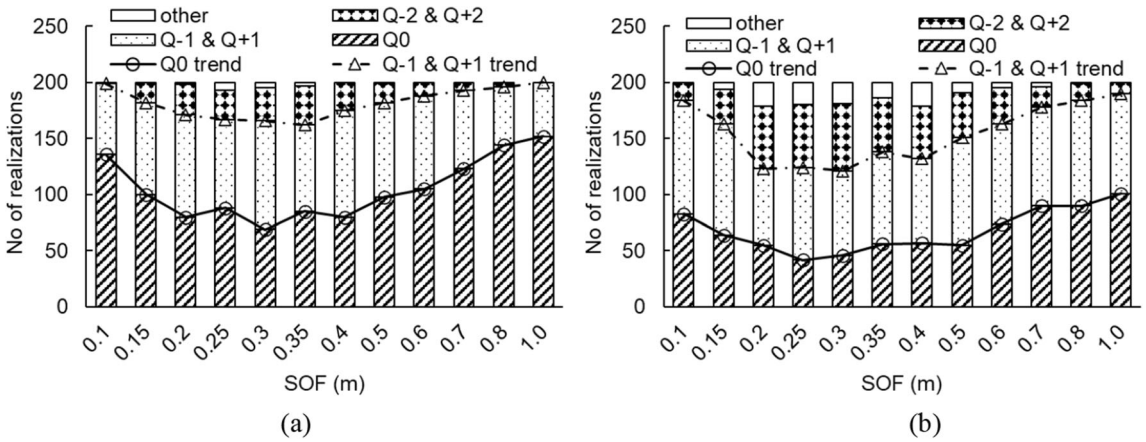

Fig. 7 Distribution of $\varepsilon_v^{\text{sub}}$ at different locations for different SOF under **a** COV_E= 0.3 and **b** COV_E= 0.5

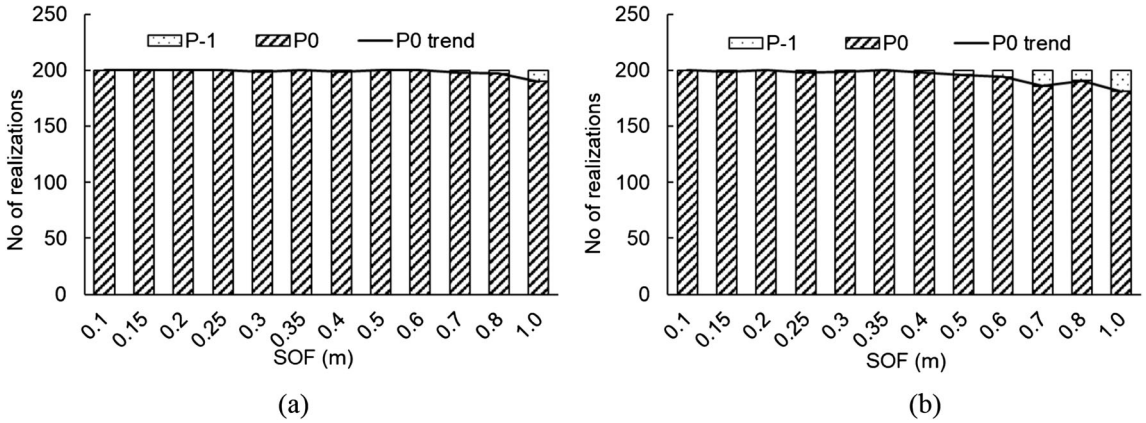

Fig. 8 Distribution of ε_h^{ac} at different locations for different SOF under **a** COV_E= 0.3 and **b** COV_E= 0.5

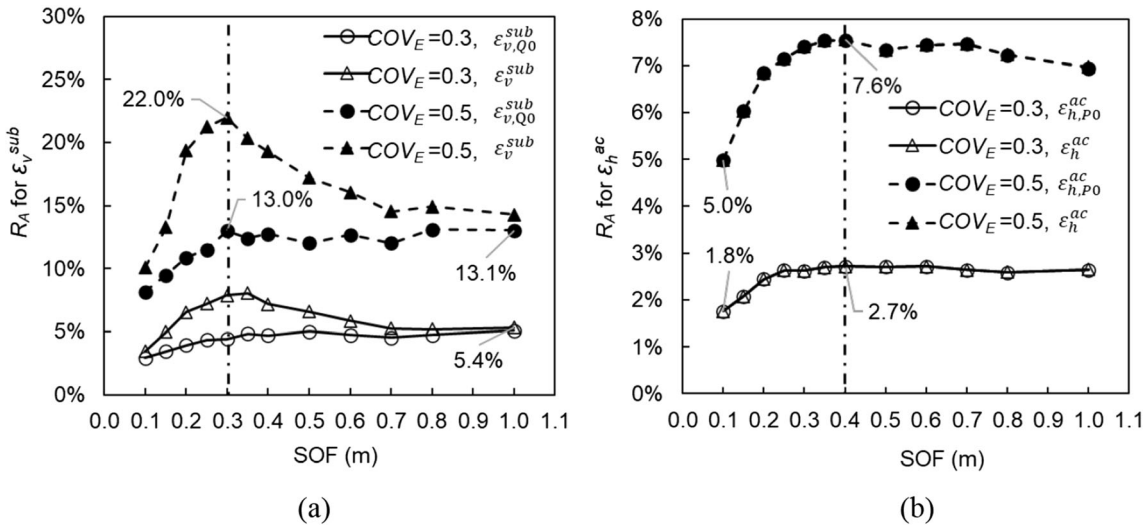

Fig. 9 Variation of R_A for **a** $\varepsilon_v^{\text{sub}}$ and **b** $\varepsilon_h^{\text{ac}}$ with increasing SOF under different values of COV_E

subgrade modulus. Moreover, the COV of $\varepsilon_v^{\text{sub}}$ exhibits much higher values and displays a distinct trend with SOF compared to that of $\varepsilon_h^{\text{ac}}$. Specifically, the COV of $\varepsilon_v^{\text{sub}}$ initially rises with increasing SOF and peaks at SOF = 0.3 m, after which it stabilizes. On the other hand, the COV of $\varepsilon_h^{\text{ac}}$ generally increases with SOF, but the impact of

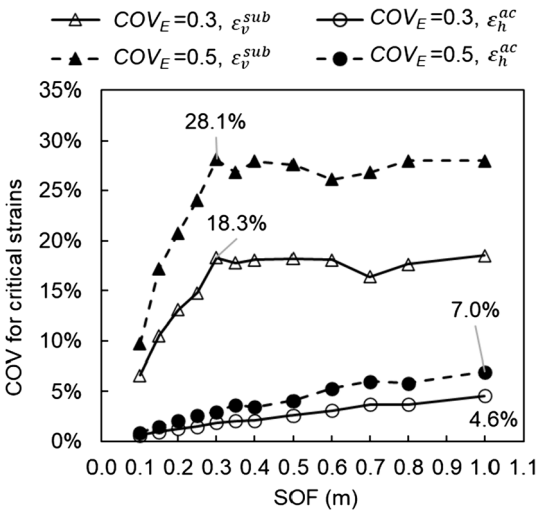

Fig. 10 Variation of COV for critical strains with increasing SOF under different values of COV_E

subgrade spatial variability is negligible for small SOF values due to the spatial averaging effect. Notably, the COVs for both ε_h^{ac} and ε_v^{sub} are considerably smaller compared to COV_E. For example, for $COV_E = 0.5$, COV for ε_h^{ac} is below 7% and COV for ε_v^{sub} is below 30%. The findings suggest a reduction of uncertainty during the uncertainty propagation from material properties to structural performance. So, in a probabilistic analysis of pavements that incorporates spatial variability, it is inappropriate to directly equate the COV of material properties with the COV of critical structural responses.

3.1.4 The maximum and minimum critical strains

The extreme values, i.e., the maximum and minimum critical strains, depict the range of distribution and provide insight into the dispersion of critical strains in probabilistic analysis. To assess the relative deviation of these extreme values from the deterministic strains, two deviation ratios, $R_{D,\max}$ and $R_{D,\min}$, are introduced. These ratios are calculated as follows:

$$R_{D,\max} = \varepsilon_{\max}/\varepsilon_{\det} - 1 \quad (6)$$

$$R_{D,\min} = 1 - \varepsilon_{\min}/\varepsilon_{\det} \quad (7)$$

where $\varepsilon_{\max}$ and $\varepsilon_{\min}$ correspond to the maximum and minimum critical strains observed in a specific case.

Figure 11 depicts the variations of $R_{D,\max}$ and $R_{D,\min}$ for the critical strains as SOF increases at different values of COV_E. The figure shows that $R_{D,\max}$ consistently exceeds $R_{D,\min}$ for both ε_v^{sub} and ε_h^{ac}. For instance, when COV_E=0.3, $R_{D,\max}$ for ε_v^{sub} ranges from 24.3 to 86.1%, whereas R_{min} ranges from only 13.8% to 44.5%. Moreover, as the degree of spatial variability intensifies with higher values of COV_E, the disparity between $R_{D,\max}$ and $R_{D,\min}$ widens even further. These findings indicate that the maximum strains deviate more significantly from the deterministic strains than the minimum ones, suggesting left-skewed distributions for both ε_h^{ac} and ε_v^{sub}. Notably, a smaller ε_v^{sub} is associated with a stiffer key influence zone (KIZ), while a higher ε_v^{sub} corresponds to a softer KIZ. Hence, the left-skewed distribution of ε_v^{sub} implies that the softer KIZ has a greater impact on critical strain compared to the stiffer KIZ, a phenomenon known as the low modulus dominating effect [19]. A detailed explanation of this effect will be provided later.

Figure 11a and b also reveals notable distinctions between ε_h^{ac} and ε_v^{sub} in terms of the deviation ratios. In Fig. 11a, $R_{D,\max}$ and $R_{D,\min}$ show non-monotonic patterns as SOF increases, with the highest deviation ratios observed at intermediate levels of SOF within the predefined ranges. Conversely, in Fig. 11b, the deviation ratios of ε_h^{ac} show increasing trends with SOF. Additionally, the deviation ratios of ε_h^{ac} are significantly lower than those of ε_v^{sub} in each case. This confirms that the impact of subgrade spatial variability on critical subgrade strain significantly surpasses its effect on critical asphalt strain.

3.2 Statistical and mechanical explanation for amplifying effect and worst SOF for ε_v^{sub}

As found in Sect. 3.1, subgrade spatial variability significantly amplifies the pavement response, particularly the critical subgrade strain, ε_v^{sub}. Additionally, both the highest amplification ratio (R_{mean}) and COV for ε_v^{sub} are observed when SOF is approximately 0.3 m (i.e., 1.5*D*). This section aims to uncover the statistical and mechanical mechanisms of these observations by examining the correlations among ε_v^{sub}, E_{Local}, and the local spatial variability within the key influence zone (KIZ). Figure 12 illustrates the correlation between E_{Local} and ε_v^{sub} for Case 2–5 (SOF = 0.25 m and COV_E= 0.5). The data points are fitted using a power regression model and divided into four quadrants based on the deterministic subgrade strain (i.e., 3.71 millistrain, denoted as $\varepsilon_{v,\text{det}}^{sub}$) and deterministic subgrade modulus (i.e., 60 MPa, denoted as E_{det}). The number of data points in each quadrant is shown in the figure. Additionally, the results from 200 deterministic analyses are included, encompassing subgrade moduli ranging from 20 to 150 MPa.

In Fig. 12, the critical subgrade strain ε_v^{sub} demonstrates an increasing trend as E_{Local} decreases in spatial variable situations, which is consistent with the deterministic situations. However, despite the statistical equivalence of the subgrade modulus between spatially variable and

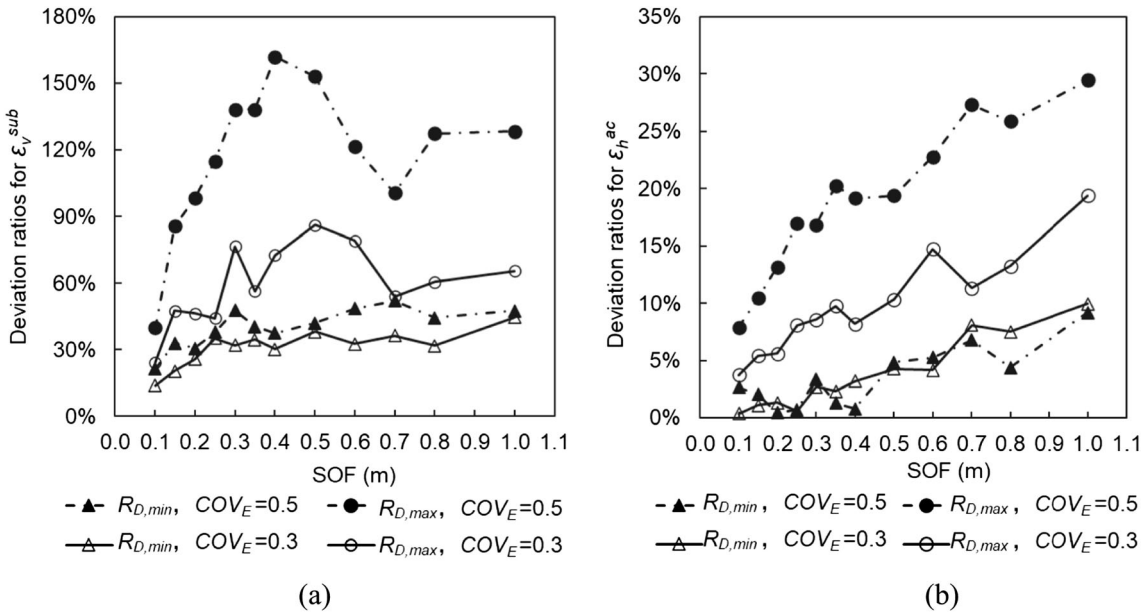

Fig. 11 Variation of deviation ratios for **a** $\varepsilon_v^{\text{sub}}$ and **b** $\varepsilon_h^{\text{ac}}$ with increasing SOF under different values of COV_E

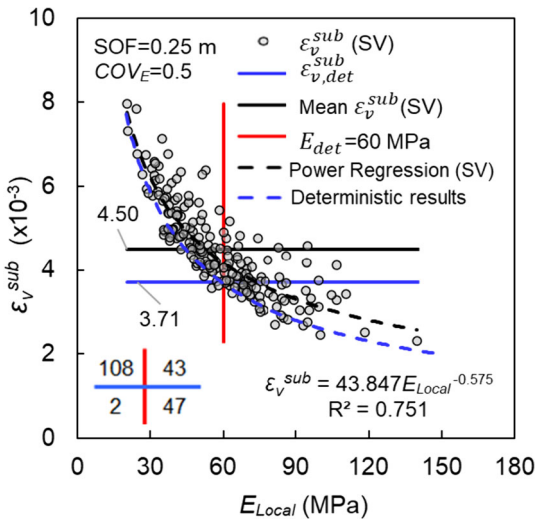

Fig. 12 Correlation between E_{Local} and $\varepsilon_v^{\text{sub}}$ for Case 2–5 (SOF = 0.25 m, and COV_E = 0.5)

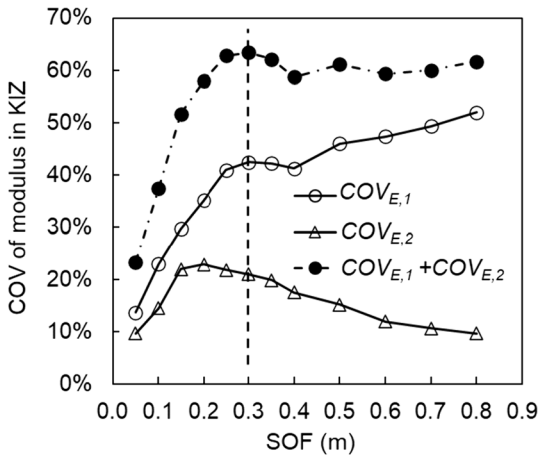

Fig. 13 Effects of SOFs on $\text{COV}_{E,1}$ and $\text{COV}_{E,2}$

deterministic cases, the number of realizations with $\varepsilon_v^{\text{sub}}$above $\varepsilon_{v,\text{det}}^{\text{sub}}$ far exceeds the number below $\varepsilon_{v,\text{det}}^{\text{sub}}$. Among 200 realizations, $\varepsilon_v^{\text{sub}}$exceeds $\varepsilon_{v,\text{det}}^{\text{sub}}$ in 151 realizations. Specifically, for realizations with $E_{\text{Local}} \leq E_{\text{det}}$, 98% of $\varepsilon_v^{\text{sub}}$ is greater than $\varepsilon_{v,\text{det}}^{\text{sub}}$, while for realizations with $E_{Local} > E_{det}$, 48% of them still exhibit $\varepsilon_v^{\text{sub}}$ higher than $\varepsilon_{v,\text{det}}^{\text{sub}}$. Consequently, the number of realizations with $\varepsilon_v^{\text{sub}}$ above $\varepsilon_{v,\text{det}}^{\text{sub}}$ (i.e., 151) significantly surpasses that with E_{Local} below E_{det}(i.e., 110). This discrepancy is due to the combined impact of the low modulus dominating effect and the local spatial variability within the KIZ. As discussed by Fenton and Griffiths [19], the low modulus dominating effect indicates that the softer regions exert a greater influence on critical strain compared to the stiffer regions. This claim is also supported by the power regression trend observed in Fig. 12, where $\varepsilon_v^{\text{sub}}$ increases at an accelerating rate with decreasing E_{Local}. It is worth noting that even when E_{Local} is very close in certain realizations, the corresponding $\varepsilon_v^{\text{sub}}$ can exhibit substantial variations. This can be attributed to the local spatial variability within the KIZ. Generally, a substantial degree of local spatial variability intensifies the low modulus dominating effect, consequently exacerbating the impairment of the deformation resistance of the KIZ.

To further explore the mechanical and statistical reasons behind the varying impact of subgrade spatial variability

for different SOF, the coefficient of variation of E_{Local} (denoted as $\text{COV}_{E,1}$) and the average coefficient of variation for the moduli (denoted as $\text{COV}_{E,2}$) in the six meshes of the KIZ (Fig. 4) are plotted against SOF in Fig. 13. Note that $\text{COV}_{E,2}$ quantifies the extent of local spatial variability within the KIZ. Figure 13 shows that $\text{COV}_{E,1}$ rapidly increases with SOF when SOF < 0.25 m and reaches its maximum at SOF = 0.3 m. Subsequently, $\text{COV}_{E,1}$ gradually approaches the coefficient of variation in the subgrade modulus (i.e., COV_E=0.5). As for $\text{COV}_{E,2}$, it exhibits a swift increase with SOF when SOF < 0.15m and reaches its maximum at SOF = 0.15 m. Afterward, $\text{COV}_{E,2}$ gradually declines with increasing SOF. Although $\text{COV}_{E,1}$ and $COV_{E,2}$ cannot reach their respective maximum at the same SOF due to their different trends, their combined value reaches its maximum at SOF = 0.3 m. Therefore, the SOF of 0.3 m signifies a situation where both the variation of E_{Local} and the local spatial variability within the KIZ are notably significant. Consequently, this explains why an SOF value of 0.3 m induces the most unfavorable effect on $\varepsilon_v^{\text{sub}}$, such as the maximum amplification ratio and the highest variability.

Notably, all the statistics of $\boldsymbol{\varepsilon_h^{ac}}$, especially the COVs and the extreme values (as shown in Fig. 10 and Fig. 11), display a similar trend to that of $\text{COV}_{E,1}$ as SOF increases. This similarity can be attributed to the spatial averaging effect, which smooths out the local variations in the KIZ. Consequently, the effect of subgrade spatial variability on $\boldsymbol{\varepsilon_h^{ac}}$ is primarily governed by $\text{COV}_{E,1}$ rather than $\text{COV}_{E,2}$.

3.3 Effect of subgrade spatial variability on the effectiveness of geogrid reinforcement

3.3.1 Difference of the effectiveness of geogrid between deterministic and spatially variable scenarios

Previous studies have shown that geogrid reinforcement in pavements can alleviate critical pavement strains, as evidenced by laboratory tests and deterministic numerical simulations [8, 12, 23]. It is reasonable to expect that these benefits can also apply to situations involving subgrade spatial variability This section compares the effectiveness of geogrid reinforcement between deterministic and spatially variable scenarios. The objective is to investigate whether subgrade spatial variability enhances or reduces the efficacy of geogrid reinforcement in reducing critical strains. To achieve this, further analysis was conducted based on Case 2–2 (SOF = 0.25 m, COV_E=0.5) from Table 3. Six types of geogrid reinforcement (G1_L1, G2_L1, G1_L1-2, G2_L1-2, G1_L2, G2_L2) will be evaluated. For brevity, G_L1 refers to geogrid reinforcement positioned at the interface between the asphalt and base layer, and similar nomenclature applies to the other configurations. To evaluate the effectiveness of geogrid in reducing critical strains, a strain alleviating ratio (*SAR*) is defined as the percentage of critical strain reduction achieved by the geogrid reinforcement. A higher value of *SAR* indicates a greater ability of the geogrid reinforcement to alleviate critical strains.

Figure 14 shows the variation of mean *SAR* under different geogrid conditions in both deterministic and spatially variable scenarios. The results indicate that, regardless of subgrade spatial variability, G_L1 performs better in reducing $\varepsilon_h^{\text{ac}}$ compared to $\varepsilon_v^{\text{sub}}$. Conversely, G_L1-2 exhibits good performance in reducing both $\varepsilon_h^{\text{ac}}$ and $\varepsilon_v^{\text{sub}}$. In comparison, G_L2 is more effective in reducing $\varepsilon_v^{\text{sub}}$ than $\varepsilon_h^{\text{ac}}$. Comparing the results of deterministic and spatially variable scenarios reveals that the strain-alleviating ability of the geogrids is greatly affected by subgrade spatial variability, and the nature and level of the influence depend on the type of critical strain and the placement position of the geogrid. Figure 14a shows that due to the subgrade spatial variability, the effectiveness of G_L1 in reducing $\varepsilon_h^{\text{ac}}$ is slightly promoted while G_L1-2 and G_L2 are slightly undermined. Figure 14b indicates, due to the subgrade spatial variability, that the effectiveness of G_L1 in reducing $\varepsilon_v^{\text{sub}}$ is slightly enhanced, while geogrids placed at the other two positions, particularly G_L2, are significantly impaired. Specifically, in the deterministic case, G1_L2 reinforcement reduces $\varepsilon_v^{\text{sub}}$ by 20.6%, whereas in spatially variable cases, the reduction is only 10.9%. Furthermore, the stiffer for G_L1-2 and G_L2, the greater the difference in their ability to reduce $\varepsilon_v^{\text{sub}}$ between the deterministic and spatially variable scenarios.

3.3.2 Statistical and mechanical explanation for the detrimental impact of subgrade spatial variability on the effectiveness of G_L2

Figure 15 depicts the relationship between E_{Local} and the strain alleviating ratio (*SAR*) of G1_L2 reinforcement for $\varepsilon_v^{\text{sub}}$. It reveals the *SAR* values of most realizations (187 out of 200) in the spatially variable scenario are lower than the deterministic value (i.e., 20.6%, denoted as $\varepsilon_{v,\text{det}}^{\text{sub}}$). Moreover, among the 200 realizations, 110 of them have E_{Local} lower than E_{det}, and 2.7% of those (3/110 = 2.7%) have a *SAR* value higher than SAR_{det}. On the other hand, in the remaining 90 realizations with E_{Local} greater than E_{det}, 11.1% of them (10/90 = 11.1%) have a *SAR* value higher than SAR_{det}. These findings suggest that as the key influence zone (KIZ) becomes stiffer, there is an increased probability of the *SAR* value being higher than the

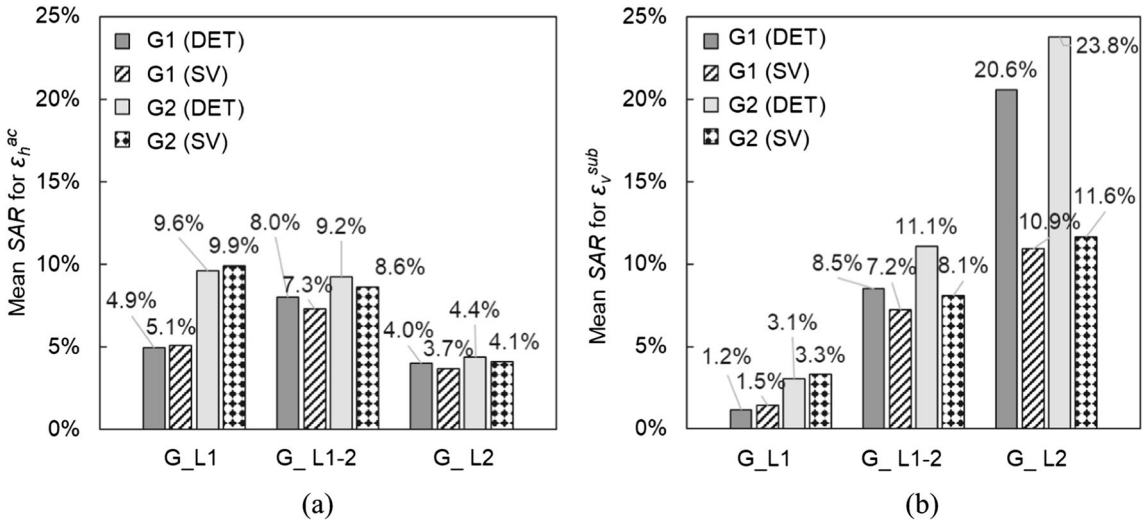

Fig. 14 Mean *SAR* of **a** ε_h^{ac} and **b** ε_v^{sub} under different geogrid reinforcement schemes

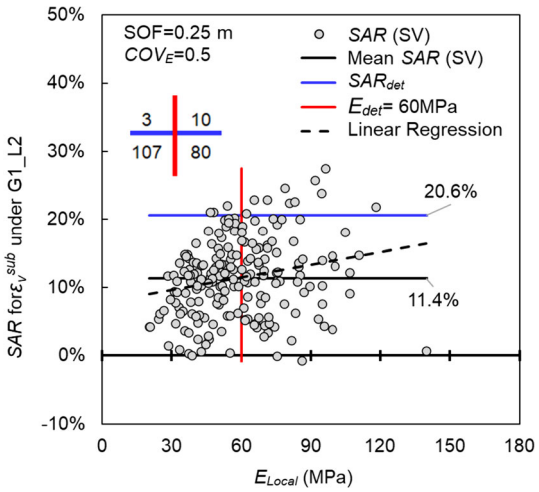

Fig. 15 Relationship of *SAR* for ε_v^{sub} versus E_{Local} under G1_L2 reinforcement

deterministic value, which is also supported by the linear regression trend in Fig. 15. This implies that a higher subgrade modulus, especially within the KIZ, enhances the capacity of G_L2 to reduce critical subgrade strains.

In general, it has been widely reported [16, 43] that large deformations facilitate the mobilization of geogrid reinforcement and improve the performance of reinforced pavement. However, the amplified critical subgrade strains observed in this study do not result in greater strain alleviating effects of G_L2 compared to the deterministic case. One possible explanation is that the locally weak KIZ not only induces greater subgrade strains but also alters the magnitude of stresses transmitted to the KIZ or the base course–subgrade interface, which might negatively affect the geogrid performance. To verify this hypothesis, the average stress transmitted to the top of KIZ (σ_v^{sub}) was computed, and its relationship with E_{Local} and the strain alleviating ratio (*SAR*) are demonstrated in Fig. 16. Figure 16a shows that, in most realizations (154 out of 200), σ_v^{sub} is lower than the deterministic value (i.e., $\sigma_{v,det}^{sub}$). Specifically, for realizations with $E_{Local} \leq E_{det}$, 100 out of 110 have σ_v^{sub} lower than $\sigma_{v,det}^{sub}$, whereas for the other 90 realizations with $E_{Local} > E_{det}$, 54 of them have σ_v^{sub} higher than $\sigma_{v,det}^{sub}$. Consequently, the number of realizations with σ_v^{sub} below $\sigma_{v,det}^{sub}$ (154 out of 200) is significantly higher than the number of realizations with E_{Local} below E_{det}(110 out of 200). This indicates that a softer and spatial variable KIZ reduces the vertical pressure transmitted to the top of KIZ. Mechanically, this can be attributed to the fact that a softer KIZ induces higher vertical subgrade strain, causing more vertical stress to be transmitted to the relatively stiffer area outside the KIZ, and eventually resulting in reduced σ_v^{sub}. Note that this reduction in σ_v^{sub} in turn mitigate the large subgrade strain, but not to the extent of fully reversing the strain amplifying effect of subgrade spatial variability.

Figure 16b indicates an increasing trend of *SAR* with increasing σ_v^{sub}For the 154 realizations with σ_v^{sub} lower than the deterministic value ($\sigma_{v,det}^{sub}$), only 3.9% have a *SAR* higher than SAR_{det} (i.e., 20.6%), while for the other 46 realizations with $\sigma_v^{sub} > \sigma_{v,det}^{sub}$, 15% of them have a *SAR* higher than SAR_{det}. Figures 15 and 16b collectively indicate that high levels of strain and stress in the proximity of base course–subgrade improve the strain-alleviating ability of G1_L2, which is in accordance with previous studies [16, 43]. However, in the context of subgrade spatial variability, the adverse impact of reduced vertical stress at the base course–subgrade interface outweighs the positive effect of the amplified subgrade strain. Consequently, the

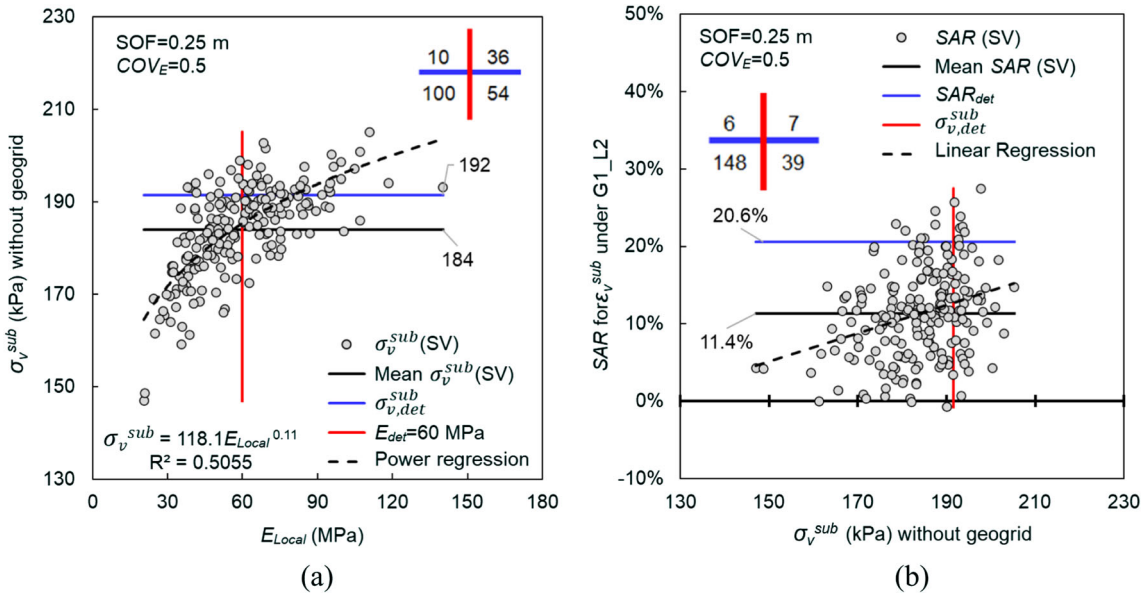

Fig. 16 Relationship of σ_v^{sub} with **a** E_{Local} and **b** *SAR* for $\varepsilon_v^{\text{sub}}$ under G1_L2 reinforcement

strain-alleviating ability of G1_L2 is generally compromised. Furthermore, out of the 46 realizations with $\sigma_v^{\text{sub}} > \sigma_{v,\text{det}}^{\text{sub}}$, only 7 realizations have a *SAR* higher than SAR_{det}. This discrepancy can be attributed to the local spatial variability within KIZ. When the subgrade modulus changes abruptly over a short distance, considerable differential deformation or fluctuation of the subgrade surface occurs. This will adversely affect the generation of the membrane effects in the reinforcements, ultimately undermining the strain-alleviating ability of G1_L2.

Overall, when geogrids are placed within or at the bottom of base course, their strain-alleviating ability is negatively affected by the subgrade spatial variability. This finding has practical implications, particularly when the subgrade layer exhibits significant spatial variation. To counteract or compensate for the negative effects caused by the subgrade spatial variability on geogrid effectiveness, measures such as using stronger geogrids or implementing treatments like surface subgrade material replacement and stabilization should be considered.

4 Conclusions and discussions

The subgrade modulus is one of the most crucial factors in determining pavement thickness, composition, and performance. However, the subgrade modulus can vary spatially, leading to detrimental effects on pavement performance. This study employs random field finite difference analysis (RFFDA) to examine the impact of subgrade modulus spatial variability on two critical pavement strains: the critical asphalt strain ($\varepsilon_h^{\text{ac}}$) and critical subgrade strain (σ_v^{sub}). A parametric study was conducted on two key influencers: the coefficient of variation (COV_E) and the scale of fluctuation (SOF) of the subgrade modulus. To uncover the statistical and mechanical mechanisms underlying the impact of subgrade spatial variability, the correlations between ε_v^{sub}, the overall modulus (E_{Local}) of the key influence zone (KIZ), and the local spatial variability within the KIZ were analyzed. The study also explores the influence of subgrade modulus spatial variability on the effectiveness of geogrid in reducing critical strains, considering two kinds of geogrid stiffness and three placement positions: asphalt–base course interface (L1), mid-depth of base course (L1-2) and base course–subgrade interface (L2). The geogrid's efficacy in reducing critical strains was measured by a strain alleviating ratio (*SAR*), which describes the reduction of the critical strains induced by the geogrid reinforcement. The key findings are as follows:

1. The spatial variability of the subgrade modulus can have a substantial amplifying effect on critical pavement strains. Specifically, compared to the homogeneous cases, at $\text{COV}_E = 0.5$, the critical subgrade strains can increase by 10–22% depending on the SOF. This finding suggests that assuming subgrade homogeneity can lead to an underestimation of the critical subgrade strain and, consequently, an overestimation of pavement life.
2. Subgrade spatial variability introduces considerable uncertainties in critical strains, posing a significant challenge for predicting pavement life. Furthermore, the coefficients of variation (COV) of the critical

strains are lower than COV_E, which implies a reduction of uncertainty during the uncertainty transmission from material properties to structural performance. Thus, when performing probabilistic analysis that incorporates spatial variability, the COV of material properties cannot be directly used as the COV of structural response.

3. Subgrade spatial variability also induces notable variation in the location of maximum pavement strains. The extent of this variability is influenced by the magnitudes of SOF and COV_E, and the specific type of critical strains. Therefore, assuming fixed locations for maximum strains can underestimate critical strains, as it fails to account for the possibility of maximum strains occurring at different locations than those observed in deterministic scenarios.
4. The impact of subgrade spatial variability on ε_v^{sub} is more direct and pronounced compared to its effect on ε_h^{ac} due to the spatial averaging effect. Subgrade spatial variability leads to a greater amplifying effect, higher values of COV, and increased variation of the critical position for ε_v^{sub} compared to ε_h^{ac}. Additionally, for ε_v^{sub}, there exists a worst value of SOF (i.e., 1.5*D*) that results in the most unfavorable statistical effect. In contrast, for ε_h^{ac}, the maximum mean value is observed when SOF is approximately 2*D*, while its COV and extreme values show an increasing trend as SOF increases. These findings also imply that subgrade spatial variability has a more significant impact on the pavement's rutting life compared to its fatigue life.
5. The strain-alleviating ability of the geogrids is impacted by subgrade spatial variability, with the impact varying based on the type of critical strain and geogrid location. When positioned at L1, the strain-alleviating ability of geogrid is enhanced, while geogrids placed at the other two positions (G_L1-2 or G_L2), are apparently impaired. Particularly, the mean values of *SAR* of G_L2 for ε_v^{sub} in spatially variable situations are only half of those observed in deterministic scenarios. Furthermore, as geogrid stiffness increases, the disparity in the ability of G_L1-2 and G_L2 in reducing ε_v^{sub} between deterministic and spatially variable scenarios becomes more pronounced. These findings imply that when the geogrid is positioned within or at the bottom of a base course, measures such as employing stronger geogrids or implementing specialized soil treatments should be taken to compensate for the adverse effects arising from subgrade spatial variability.
6. The influence of subgrade spatial variability on the statistics of critical strains can be attributed to the low modulus dominating effect, which depends on two factors: E_{Local} and the local spatial variability within the KIZ. A KIZ with lower E_{Local} and higher local spatial variability results in reduced deformation resistance, leading to higher ε_v^{sub} but lower vertical stress transmitted to the KIZ. Higher level of strain or stress tends to improve the strain-alleviating ability of geogrid. However, for G_L2, the negative effect of the reduced vertical stress outweighs the positive effect of the amplified subgrade strain. Consequently, the ability of G_L2 in reducing ε_v^{sub} is compromised.

Pavement design methods employ the reliability concept to compensate for variations and uncertainties in material properties and loading conditions. This study quantified the influence of subgrade spatial variability on the two kinds of critical strains: ε_h^{ac} and ε_v^{sub}. Since ε_h^{ac} and ε_v^{sub} are closely linked to the pavement fatigue life and rutting life, respectively, the influence of subgrade spatial variability on both fatigue and rutting life can also be assessed. The impact of asphalt spatial variability on critical strain and pavement life has recently been explored by the authors [41]. The effect of spatial variability in the base course remains under-researched and will be addressed in future. All these studies necessitate further study on the coupling effects of spatial variability across multiple pavement layers and facilitate a more advanced and refined reliability-based design to better capture the spatial variability-induced uncertainties. Of course, to systematically integrate spatial variability with established reliability principles, further research is required to ensure accurate probabilistic characterization of material spatial variability for natural soil and man-made asphalt layer.

Acknowledgements The first author received PhD scholarships from the University of New South Wales and the Australian Government Research Training Program. The project is funded by the ARC Industrial Transformation Research Hub Project Grant—IH180100010 (Project No. IH18.09.1 and IH18.09.2).

Funding Open Access funding enabled and organized by CAUL and its Member Institutions.

References

1. AASHTO (2008) Mechanistic-empirical pavement design guide: a manual of practice. Washington, DC, USA
2. Abu-Farsakh M et al (2007) Effect of soil moisture content and dry density on cohesive soil–geosynthetic interactions using large direct shear tests. J Mater Civ Eng 19(7):540–549
3. Alhasan A, Ali A, Offenbacker D, Smadi O, Lewis-Beck C (2018) Incorporating spatial variability of pavement foundation layers stiffness in reliability-based mechanistic-empirical pavement performance prediction. Transp Geotech 17:1–13
4. Ali AW, Abbas AR, Nazzal M, Sett K (2013) Incorporation of subgrade modulus spatial variability in performance prediction of flexible pavements. Int J Pavement Res Technol 6(2):136–140
5. Al-Jumaili M (2016) Finite element modelling of asphalt concrete pavement reinforced with geogrid by using 3-D plaxis software. Int J Mater Chem Phys 2(2):62–70
6. Arsenie IM et al (2017) Modelling of the fatigue damage of a geogrid-reinforced asphalt concrete. Road Mater Pavement Design 18(1):250–262
7. Austroads (2017) Guide to Pavement technology part 2: pavement structural design. Austroads, Sydney, Australia
8. Cami B et al (2020) Scale of fluctuation for spatially varying soils: estimation methods and values. ASCE-ASME J Risk Uncertain Eng Syst Part A Civ Eng 6(4):03120002
9. Cancelli A, Montanelli F, Rimoldi P, Zhao A (1997) Full scale laboratory testing on geosynthetics reinforced paved roads. In Proc. of the International Symposium on Earth Reinforcement
10. Canestrari F, Belogi L, Ferrotti G, Graziani A (2015) Shear and flexural characterization of grid-reinforced asphalt pavements and relation with field distress evolution. Mater Struct 48(4):959–975
11. Chen L et al. (2023) Efficient numerical-simulation-based slope reliability analysis considering spatial variability. Acta Geotechnica
12. Ching JY, Hu YG (2016) Effect of element size in random finite element analysis for effective young's modulus. Math Probl Eng 2016(1):1–10
13. Choudhuri K, Chakraborty D (2021) Probabilistic bearing capacity of a pavement resting on fibre reinforced embankment considering soil spatial variability. Front Built Environ 2021(7):628016
14. Correia NS, Mugayar AN (2021) Effect of binder rates and geogrid characteristics on the shear bond strength of reinforced asphalt interfaces. Constr Build Mater 269:121292
15. Correia NS, Zornberg JG (2016) Mechanical response of flexible pavements enhanced with geogrid-reinforced asphalt overlays. Geosynth Int 23(3):183–193
16. Correia NS, Esquivel ER, Zornberg JG (2018) Finite-element evaluations of geogrid-reinforced asphalt overlays over flexible pavements. J Transp Eng Part B-Pavements 144(2)
17. Cuelho EV, Perkins SW (2005) Resilient interface shear modulus from short-strip, cyclic pullout tests. In slopes and retaining structures under seismic and static conditions (pp. 1–11)
18. Fathi A et al. (2020) Correlating continuous compaction control measurements to in situ modulus-based testing for quality assessment of compacted geomaterials. 3rd International Conference on Information Technology in Geo-Engineering (ICITG), Guimaraes, PORTUGAL
19. Fenton GA, Griffiths DV (2005) Three-dimensional probabilistic foundation settlement. J Geotech Geoenviron Eng 131(2):232–239
20. Gong WP, Tang HM, Juang CH, Wang L (2020) Optimization design of stabilizing piles in slopes considering spatial variability. Acta Geotech 15(11):3243–3259
21. Gu F, Luo X, Luo R, Lytton RL, Hajj EY, Siddharthan RV (2016) Numerical modeling of geogrid-reinforced flexible pavement and corresponding validation using large-scale tank test. Constr Build Mater 122:214–230
22. He X et al (2022) Deep learning for efficient stochastic analysis with spatial variability. Acta Geotech 17(4):1031–1051
23. Huang HW, Xiao L, Zhang DM, Zhang J (2017) Influence of spatial variability of soil Young's modulus on tunnel convergence in soft soils. Eng Geol 228:357–370
24. Huang JS, Lyamin AV, Griffiths DV (2013) Quantitative risk assessment of landslide by limit analysis and random fields. Comput Geotech 53:60–67
25. Huang SP, Quek ST, Phoon KK (2001) Convergence study of the truncated Karhunen-Loeve expansion for simulation of stochastic processes. Int J Numer Anal Methods Geomech 52(9):1029–1043
26. Ling HI, Liu HB (2003) Finite element studies of asphalt concrete pavement reinforced with geogrid. J Eng Mech 129(7):801–811
27. Lua YJ, Sues RH (1996) Probabilistic finite-element analysis of airfield pavements. Transportation Research Record 1540, Transportation Research Board, National Research Council, Washington, DC, 29–38
28. Luo Z et al (2018) Effect of uncertain material property on system reliability in mechanistic-empirical pavement design. Constr Build Mater 172:488–498
29. Mamatha KH, Dinesh SV (2019) Effectiveness of geogrid and its position on the performance of unpaved roads under repetitive loading. Innov Infrastruct Sol 4(1):62
30. McCartney JS et al (2009) Analysis of a large database of GCL-geomembrane interface shear strength results 135(2):209–223
31. Perkins SW (2001). Mechanistic–empirical modeling and design model development of geosynthetic reinforced flexible pavements. Rep. No. FHWA/MT-01- 002/99160-1A. Helena, Montana: Montana Dept. of transportation
32. Phoon KK, Kulhawy FH (1999) Characterization of geotechnical variability. Can Geotech J 36(4):612–624
33. Rahman A et al (2017) State-of-the-art review of interface bond testing devices for pavement layers: toward the standardization procedure. J Adhes Sci Technol 31(2):109–126
34. Sudarsanan N et al (2018) An investigation on the interface bond strength of geosynthetic-reinforced asphalt concrete using Leutner shear test. Constr Build Mater 186:423–437
35. Sudarsanan N, Arulrajah A, Karpurapu R, Amirthalingam V (2020) Fatigue performance of geosynthetic-reinforced asphalt concrete beams. J Mater Civ Eng 32(8)
36. Timm D, Newcomb D, Galambos T (2000) Incorporation of reliability into mechanistic-empirical pavement design. Transp Res Rec 1730:73–80
37. Vaillancourt M, Houy L, Perraton D, Breysse D (2014) Variability of subgrade soil rigidity and its effects on the roughness of flexible pavements: a probabilistic approach. Mater Struct 48(11):3527–3536
38. Vanmarcke E (2010) Random fields: analysis and synthesis. World scientific
39. Webster SL (1993) Geogrid reinforced base courses for flexible pavements for light aircraft: test section construction, behavior under traffic, laboratory tests, and design criteria
40. White DJ, Vennapusa P, Tutumluer E, Vavrik W, Moaveni M, Gillen S (2018) Spatial verification of modulus for pavement foundation system 2672(52):333–346
41. Xiao L, Xue J (2023) Effect of spatial variability in asphalt layer on critical pavement strains. Constr Build Mater 408:133789
42. Zhang DM et al. (2023) Bearing capacity of shallow foundations considering geological uncertainty and soil spatial variability. Acta Geotechnica
43. Zornberg JG (2017) Functions and applications of geosynthetics in roadways. Procedia Eng 189:298–306